JOURNAL OF VIROLOGY, July 2007, p. 7504–7516 Vol. 81, No. 14
0022-538X/07/$08.00+0 doi:10.1128/JVI.02690-06

Poliovirus Induces Bax-Dependent Cell Death Mediated by c-Jun NH_2-Terminal Kinase▽

Arnaud Autret,[1] Sandra Martin-Latil,[1] Laurence Mousson,[1] Aurélie Wirotius,[1] Frédéric Petit,[2] Damien Arnoult,[2] Florence Colbère-Garapin,[1] Jérôme Estaquier,[2]† and Bruno Blondel[1]*

Biologie des Virus Entériques[1] and Unité de Physiopathologie des Infections Lentivirales,[2] Institut Pasteur, 75724 Paris, France

Received 6 December 2006/Accepted 30 April 2007

Poliovirus (PV) is the causal agent of paralytic poliomyelitis, a disease that involves the destruction of motor neurons associated with PV replication. In PV-infected mice, motor neurons die through an apoptotic process. However, mechanisms by which PV induces cell death in neuronal cells remain unclear. Here, we demonstrate that PV infection of neuronal IMR5 cells induces cytochrome *c* release from mitochondria and loss of mitochondrial transmembrane potential, both of which are evidence of mitochondrial outer membrane permeabilization. PV infection also activates Bax, a proapoptotic member of the Bcl-2 family; this activation involves its conformational change and its redistribution from the cytosol to mitochondria. Neutralization of Bax by vMIA protein expression prevents cytochrome *c* release, consistent with a contribution of PV-induced Bax activation to mitochondrial outer membrane permeabilization. Interestingly, we also found that c-Jun NH_2-terminal kinase (JNK) is activated soon after PV infection and that the PV-cell receptor interaction alone is sufficient to induce JNK activation. Moreover, the pharmacological inhibition of JNK by SP600125 inhibits Bax activation and cytochrome *c* release. This is, to our knowledge, the first demonstration of JNK-mediated Bax-dependent apoptosis in PV-infected cells. Our findings contribute to our understanding of poliomyelitis pathogenesis at the cellular level.

Poliovirus (PV), the etiological agent of paralytic poliomyelitis, is a member of the genus *Enterovirus* belonging to the *Picornaviridae* family, a family that contains many human and animal pathogens (56). Despite the success of the World Health Organization's program for the global eradication of poliomyelitis, PV remains a public health issue. This is due in part to the rapid spread of PV in insufficiently immunized populations and to the emergence of epidemic vaccine-derived PV, threatening to undermine the eradication program (32).

PV is composed of a single-stranded RNA genome of positive polarity surrounded by a nonenveloped icosahedral protein capsid. The capsid consists of 60 copies of each of the four viral structural proteins, VP1 to VP4. A deep surface depression, called the canyon, surrounds each fivefold axis of symmetry and contains the site for cell receptor binding. The human PV receptor, CD155, and its simian counterparts are members of the immunoglobulin superfamily (36, 37, 50). They are related to the nectin family of adhesion molecules (46, 67).

PV is transmitted mainly via the fecal-oral route. It first infects the oropharynx and the digestive tract and then spreads to the central nervous system, in which it mostly targets motor neurons, and the death of these cells leads to paralysis. The process by which neurons are killed was unknown until recently (52, 61). Work with mouse models has shown that PV-infected motor neurons in the spinal cord die by apoptosis: the extent of apoptosis correlates with the viral load, and its onset coincides with that of paralysis (10, 21). PV-induced apoptosis therefore seems to be a major contributor to the tissue injury in the central nervous system.

Apoptosis is an active process of cell death that occurs in response to various stimuli, including viral infection (64). It is mediated in particular by a family of cysteine proteases with specificity for aspartic acid residues called caspases. In numerous models, mitochondria act as a pivotal regulator of apoptosis (15, 25). Mitochondrial outer membrane permeabilization (MOMP) leads to the loss of the mitochondrial transmembrane potential and the release of proapoptotic molecules, including cytochrome *c*, from mitochondria to the cytosol. In the cytosol, cytochrome *c* forms a caspase-activating complex by interaction with Apaf-1 (apoptosis protease-activating factor-1) and procaspase-9. This event triggers caspase-9 activation and initiates the apoptotic cascade by processing caspase-3.

Apoptotic mitochondrial dysfunction is tightly regulated by the Bcl-2 family of proteins. Some, including Bcl-2 and Bcl-X_L, maintain the integrity of the mitochondria to prevent the release of cytochrome *c*, whereas others, in particular Bax and the so-called BH-3-only proteins, such as Bid and Bim, promote mitochondrial cytochrome *c* release. The mitochondrial pathway of apoptosis can also involve proapoptotic signal transduction via the c-Jun NH_2-terminal kinases (JNK) (69) that are activated when cells are exposed to various stress signals (16). The JNK pathway contributes to stress-induced apoptosis in several cell types, including pancreatic β cells (3), hepatocytes (60), and neurons (7). The involvement of JNK activation has also been described for some cases of virus-induced cell death, notably with reovirus (13), swine influenza virus (12), and coxsackievirus B3 (35), another member of the *Picornaviridae* family. JNK can induce mitochondrial dysfunction through a transcription-independent process that involves activating the proapoptotic proteins Bim and Bax or inactivat-

* Corresponding author. Mailing address: Biologie des Virus Entériques, Institut Pasteur, 28 rue du Docteur Roux, 75724 Paris cedex 15, France. Phone: 33 1.40.61.35.90. Fax: 33 1.40.61.34.21. E-mail: bblondel@pasteur.fr.

† Present address: INSERM V841, 94010 Créteil, France.

▽ Published ahead of print on 9 May 2007.

ing the antiapoptotic proteins Bcl-2 and Bcl-X_L (4, 18, 30, 33, 34, 55, 65, 76).

PV can trigger apoptosis in vitro in tissue cultures of human colon carcinoma cells (CaCo-2) (2), promonocytic cells (U937) (47), dendritic cells (71), murine L cells expressing CD155 (24, 63), and HeLa cells (8, 68) and in cultures of mixed mouse primary nerve cells (14) from the cerebral cortex of mice transgenic for CD155. Analyses of apoptotic pathways following PV infection in several cell lines have demonstrated MOMP as judged notably by cytochrome *c* release from mitochondria to the cytosol (8, 24). However, details of the mechanisms by which mitochondria are deregulated following PV infection are unknown and have not been described. Here, we report various characteristics of the PV-induced signaling cascade leading to the activation of the mitochondrial pathway in neuroblastoma IMR5 cells. We show that PV-mediated cytochrome *c* release is Bax dependent in these cells. Furthermore, early JNK activation following PV infection is required for Bax activation and mitochondrial dysfunction. Finally, we show that the PV-CD155 interaction alone is sufficient to induce JNK activation but that downstream steps are required for PV-induced apoptosis in IMR5 cells.

It is, to our knowledge, the first demonstration of Bax-dependent JNK-mediated apoptosis in PV-infected cells. Our findings contribute to a better understanding of poliomyelitis pathogenesis at a cellular level.

MATERIALS AND METHODS

Materials. (i) Chemicals. Sheep anti-cytochrome *c* (C5723) and mouse anti-actin (A3853) antibodies, staurosporine (STS) (S4400), phosphatase inhibitor cocktail (P2850), and protein G (P3296) were obtained from Sigma-Aldrich. SP600125 (420119) and z-VAD-fmk (627610) were purchased from Calbiochem. Complete protease inhibitor mixture was obtained from Roche Applied Science. Mouse anti-cytochrome oxidase subunit IV (Cox IV) (A21347) antibody, fluorescein isothiocyanate-conjugated anti-sheep (A11015) and anti-rabbit (A11070) secondary antibodies were purchased from Molecular Probes. Rabbit anti-Bax (NT 06-499) and rabbit anti-Bak (NT 06-536) antibodies were obtained from Upstate. Mouse anti-Bax (clone 6A7; sc-23959) antibody was purchased from Santa Cruz Biotechnology. Rabbit anti-Bim (AAP-330) antibody was bought from Stressgen. Horseradish peroxidase (HRP)-conjugated anti-mouse (NA9310V) and anti-rabbit (NA9340V) secondary antibodies were obtained from Amersham Biosciences. Mouse anti-cytochrome *c* (7H8.2C12) and anti-JNK1/2 (G151-666) antibodies were obtained from BD Pharmingen. Goat anti-Bid (AF860) antibody and donkey anti-goat (HAF109) HRP-conjugated antibody were purchased from Research & Diagnostic. Mouse anti-caspase-8 (9746), rabbit anti-c-Jun (9165), anti-phospho (Ser63)-c-Jun (9261) and anti-phospho (Thr183/Tyr185)-JNK (p46 [JNK1] and p54 [JNK2/3]) (9251) antibodies were purchased from Cell Signaling. Small interfering RNAs (siRNAs) that target human Bim (6461) and nontargeted siRNA (6201) were purchased from Cell Signaling.

(ii) Cell lines, virus stock, and viral infection. Human neuroblastoma IMR5 (kindly provided by S. Susin and V. Yuste, Institut Pasteur, Paris, France) and human HEp-2c cells (ATCC) were cultured in Dulbecco's modified Eagle's medium (DMEM) supplemented with 2 mM L-glutamine (Gibco) and 10% (vol/vol) heat-inactivated fetal bovine serum (FBS) (Gibco). Cells were maintained at 37°C in humidified air containing 95% air and 5% CO_2.

The attenuated vaccinal Sabin 2 strain of PV was used in this study. Virus stocks were generated in HEp-2c cells and stored at −80°C until use. Virus titers were determined on HEp-2c cells and on IMR5 cells by measuring 50% tissue culture infective dose units ($TCID_{50}$) per ml, as described by Reed and Muench (62). Virus titers in the two cell lines were similar (data not shown). In all experiments described in this study, subconfluent IMR5 cells monolayers grown in 25-cm^2 flasks (TPP) or in six-well dishes (TPP) were inoculated with PV at a multiplicity of infection (MOI) of 10 $TCID_{50}$/cell in DMEM supplemented with 10% FBS. Before PV infection, the growth medium was discarded and the virus was added to monolayers in volumes of 2 ml and 0.8 ml for 25-cm^2 flasks and six-well dishes, respectively, to provide an efficient infection. Adsorption was allowed to proceed for 30 min at 37°C in humidified air containing 5% CO_2. The cells, in flasks or in dishes, were then washed twice with serum-free medium to remove unbound particles and were then incubated with 5 ml or 2 ml, respectively, of fresh DMEM supplemented with 10% FBS at 37°C, and the virus was allowed to grow for the indicated times. Time zero postinfection (p.i.) corresponds to the inoculation time point.

In analyses of the apoptotic features of PV-infected cells, both adherent and detached cells were taken into account: attached cells were treated with EDTA and collected with detached floating cells by centrifugation for 5 min at 400 × *g*. The cells were rinsed twice by centrifugation in PBS and analyzed as described below.

UV light inactivation of PV. PV was inactivated by UV cross-linking at 6,000 μJ/cm^2 by using an Amersham UV cross-linker. Following UV irradiation, virus stocks were shown to be devoid of infectious virus by microtitration.

Assessment of apoptosis. The percentages of apoptotic cells were determined by flow cytofluorimetric analysis of aliquots of 2×10^5 cells incubated with 0.1 μg/ml acridine orange (AO) metachromatic nuclear dye (excitation wavelength, 500 nm; emission wavelength, 526 nm; Molecular Probes) for 15 min at 37°C. The AO fluorescence was measured with a FACScan (Becton Dickinson). Two populations of cells were separated, one consisting of the living cells characterized by bright fluorescence labeling and the second being apoptotic cells with a characteristic distinct pattern of reduced fluorescence intensity (20). A minimum of 10,000 cells was analyzed for each sample. Data were analyzed with Cellquest software (Becton Dickinson).

Assessment of plasma membrane integrity. The integrity of the cell plasma membrane was checked by incubating aliquots of 2×10^5 cells with 1 μg/ml propidium iodide (PI) (excitation wavelength, 535 nm; emission wavelength, 617 nm; Immunochemistry Technologies, LLC) for 15 min at 37°C. PI cannot enter cells with intact plasma membranes; when the integrity of the plasma membrane is disrupted, cells become permeable to PI (75). The percentage of cells with an intact plasma membrane was quantified by flow cytofluorimetric analysis (linear scale; FL2-A). We analyzed at least 10,000 cells for each sample. Data were analyzed with Cellquest software (Becton Dickinson).

Assessment of $\Delta\psi_m$. Changes in the mitochondrial transmembrane potential ($\Delta\psi_m$) were measured by flow cytometry analysis of aliquots of 2×10^5 IMR5 cells stained with the potential-sensitive dye 3,3′-dihexyloxacarbocyanine iodide ($DiOC_6$) (excitation wavelength, 484 nm; emission wavelength, 501 nm; Molecular Probes) for 15 min at 37°C at a final concentration of 40 nM. Loss of $DiOC_6$ staining indicates disruption of the mitochondrial membrane potential associated with apoptosis. For each sample, 10,000 cells were analyzed. Data were analyzed with Cellquest software (Becton Dickinson).

Detection of active caspase-8 and caspase-9. Caspase-8 and caspase-9 activation was assessed using carboxyfluorescein (FAM) FLICA apoptosis detection kits (Immunochemistry Technologies, LLC) according to the manufacturer's protocol. These assays are based on fluorescein-labeled inhibitors, FAM-LETD-fmk and FAM-LEHD-fmk, that bind specifically to the active forms of caspase-8 and caspase-9, respectively (excitation wavelength, 490 nm; emission wavelength, 520 nm). Apoptotic cells containing active caspase-8 and caspase-9 were detected with a FACScan (Becton Dickinson) machine. We analyzed at least 10,000 cells for each sample. Data were analyzed with Cellquest software (Becton Dickinson).

Transfection of siRNA and plasmids. RNA interference was used to silence expression of the Bim gene in IMR5 cells. Cells were plated in six-well culture dishes with complete medium and allowed to grow for 24 h to 50 to 80% confluence. Cells were transfected with siRNA that targets human Bim (6461; Cell Signaling) mRNA. A nontargeted siRNA (6201; Cell Signaling) that does not lead to the specific degradation of any cellular message was used for control experiments. A mixture of OptiMEM medium and OligofectAMINE (Invitrogen) was incubated for 10 min at room temperature and was then incubated with siRNA (50 nM) for 20 min at room temperature to allow complex formation. This mixture including siRNA was then added to each well according to the manufacturer's protocol (Invitrogen). Twelve hours after transfection, the medium was changed, and analyses were performed 72 h after transfection. Gene silencing was verified by detecting proteins by immunoblot analysis after transient transfection of IMR5 cells with siRNA. vMIA (viral mitochondrion-localized inhibitor of apoptosis) expression in IMR5 cells was used to inhibit the Bax protein conformational change (5). The OligofectAMINE (Invitrogen) reagent was used for transient transfections of IMR5 cells with mammalian expression plasmids encoding Myc-tagged vMIA and empty vector, pcDNA3.1, according to the manufacturer's protocol (Invitrogen).

Whole-cell extracts. Approximately 5×10^6 cells were collected and washed with PBS and then resuspended in lysis buffer (20 mM Tris, pH 7.5, 135 mM NaCl, 2 mM EDTA, 1% Triton X-100, 10% glycerol) supplemented with a

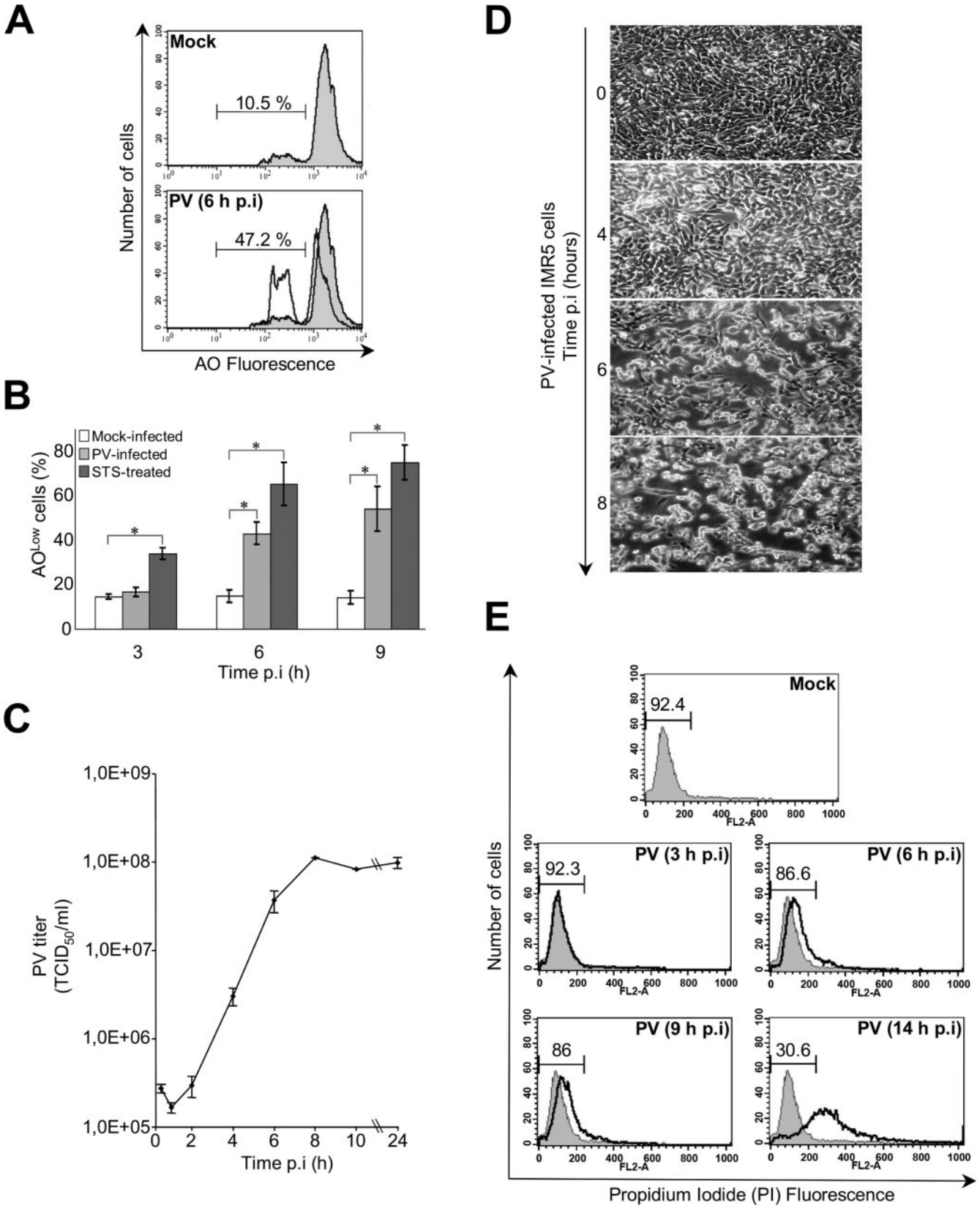

FIG. 1. PV-induced apoptosis in neuronal cells. (A) Representative flow cytometric histograms after AO nuclear dye staining of mock-infected and PV-infected (6 h p.i.) IMR5 cells. The profiles of mock-infected control cells (gray area) and PV-infected cells (blank area) are shown. The percentages of apoptotic cells corresponding to a reduced fluorescence intensity (AO^{Low}) for each of the two experimental conditions are indicated. (B) Flow cytometric analysis of PV-induced apoptosis. Mock-infected, PV-infected, and STS-treated IMR5 cells were analyzed at the indicated

protease inhibitor mixture and phosphatase inhibitor cocktail. The cells were homogenized on ice using Dounce homogenizer and incubated for 10 min at 4°C in the lysis buffer. The lysates were clarified by centrifugation for 10 min at 14,000 × *g*. The supernatant was collected as the whole-cell extract.

Subcellular fractionation. The subcellular proteome extraction kit (Calbiochem) was used to isolate cytosol and heavy membrane fractions of IMR5 cells according to the manufacturer's instructions. Aliquots of 5×10^6 cells were harvested, pelleted, washed twice, resuspended in ice-cold Extraction I buffer containing a protease inhibitor mixture and incubated for 10 min at 4°C with gentle agitation. The suspension was centrifuged at 1,000 × *g* at 4°C for 10 min. The supernatant was used as the cytosol fraction. The pellet was resuspended in ice-cold Extraction II buffer containing a protease inhibitor mixture and was incubated for 30 min at 4°C with gentle agitation. It was then centrifuged at 6,000 × *g* at 4°C, and the supernatant, the heavy membrane fraction, was collected.

Detection of Bax protein conformation change by immunoprecipitation. Cells were harvested and washed in phosphate-buffered saline (PBS) and then suspended in lysis buffer (10 mM HEPES, pH 7.4, 150 mM NaCl, 1% CHAPS {3-[(3-cholamidopropyl)-dimethylammonio]-1-propanesulfonate}) containing a mixture of protease inhibitors and a phosphatase inhibitor cocktail. The zwitterionic detergent CHAPS keeps the Bax protein in its active conformation (29). Cells were homogenized on ice in a Dounce homogenizer, incubated for 2 h in the lysis buffer, and centrifuged for 30 min at 14,000 × *g*. The resulting supernatant was incubated overnight at 4°C with 20 μl of protein G and 2 μg of the anti-Bax antibody (6A7) specific for the active conformation of Bax. The immunoprecipitates were collected by centrifugation at 1,000 × *g* (4°C, 5 min). The pellet was washed with immunoprecipitation buffer and was then suspended in 50 μl of Laemmli's buffer supplemented with reducing agent.

Western blot analysis. Protein concentrations were determined by using a protein assay kit (Bio-Rad, Richmond, CA). Samples containing equal quantities of protein were resuspended in Lammeli's electrophoresis sample buffer containing reducing agent, denatured by boiling for 5 min, and subjected to sodium dodecyl sulfate-polyacrylamide gel electrophoresis (10 to 20% Tricine gels; Novex). The proteins were then transferred to nitrocellulose membranes (Amersham Biosciences). Nonspecific sites were blocked by incubation for 1 h at room temperature with 5% nonfat milk and 0.1% Tween 20 in PBS (PBST; pH 7.4), and the membranes were incubated overnight at 4°C or 2 h at room temperature with the primary antibody. Membranes were then washed in PBST and treated with appropriate HRP-conjugated secondary antibody for 1 h at room temperature. The immunoblots were washed in PBST and proteins were revealed using an enhanced chemiluminescence detection kit (Amersham Biosciences) and autoradiography. Antiactin and Cox IV antibodies were used to verify equal protein loading. The intensities of the bands were determined by densitometry.

Cytochrome *c* and active Bax immunofluorescence staining. IMR5 cells were grown on polylysine-coated (10 μg/ml) slides and were fixed for 15 min at 4°C in paraformaldehyde (4%), and then permeabilized by treatment with 0.2% Triton X-100 in PBS for 5 min. The cells were incubated for 1 h in blocking buffer (2% bovine serum albumin in PBS) and then for 2 h at room temperature with primary antibody, a sheep anti-cytochrome *c* (Sigma) or a rabbit anti-Bax which does not recognize the nonactivated Bax (NT; Upstate). The cells were washed three times for 5 min in blocking buffer and then incubated for 2 h with Alexa Fluor secondary anti-rabbit and anti-sheep antibodies (Molecular Probes). After washes, images were acquired using a Leica DM RB microscope.

Statistical analysis. Data are expressed as means ± standard errors of the means for three independent experiments. Student's *t* test was used for comparison between experimental conditions and controls. A P value of <0.05 was considered significant.

RESULTS

MOMP in PV-infected IMR5 cells. First, we investigated the kinetics of PV-induced apoptosis and that of viral growth in IMR5 cells. Cells were infected with PV at a MOI of 10 $TCID_{50}$ per cell. Mock-infected cells, left untreated or treated with STS (2 μM), were used as positive or negative controls of apoptosis, respectively. The onset of apoptosis was analyzed 3 h, 6 h, and 9 h p.i. by measuring chromatin condensation and fragmentation by flow cytometry after AO staining of both adherent and detached cells (Fig. 1A and B). A significant proportion of cells lost AO fluorescence intensity (AO^{Low}) at 6 h p.i., and this proportion was higher 9 h p.i. (Fig. 1B). The kinetics of PV-induced apoptosis paralleled the kinetics of virus production (Fig. 1C) and the onset of cytopathic effects (the rounding and detachment of cells from the plate) (Fig. 1D). The membrane integrity of collected cells was checked by PI staining followed by flow cytometry. An intact cell membrane, often used to distinguish between apoptosis and necrosis, blocks the entry of PI into cell. When cells undergo secondary necrosis or late apoptosis, they become permeable to PI. In PV-infected cells, membrane integrity was maintained until at least 9 h p.i. (Fig. 1E). Cells became permeable to PI only much later after infection, as shown at the 14-h p.i. time point, when late apoptosis occurred or the cells were already dead. We then tested whether the $\Delta\psi_m$ collapses during PV infection. Both adherent and detached cells were treated with the fluorescent dye $DiOC_6$, and mock-infected and STS-treated IMR5 cells were used as negative and positive controls, respectively (Fig. 2A and B). Cells infected with PV exhibited a clear drop in the $\Delta\psi_m$ at 6 h (Fig. 2A) that progressed further at 9 h p.i. (Fig. 2B).

In view of the $\Delta\psi_m$ loss, we followed the kinetics of cytochrome *c* efflux from mitochondria as a surrogate indicator of MOMP in PV-infected cells. Whole-cell extracts were fractionated to separate the cytosolic fraction from the heavy membrane fraction including mitochondria. The kinetics of cytochrome *c* release was analyzed by Western blotting. Cytochrome *c* was clearly detected in the cytoplasm of infected IMR5 cells from 6 h p.i. (Fig. 2C), up to the last time point investigated (14 h p.i.). The release of cytochrome *c* from mitochondria to the cytoplasm of PV-infected IMR5 was also studied by immunofluorescence 6 h p.i. Representative staining patterns for mock-infected and PV-infected IMR5 cells are presented in Fig. 2D. The immunofluorescence staining pattern of IMR5 cells after infection with PV was diffuse, showing that cytochrome *c* was present in the cytosol; in mock-infected

times p.i. by flow cytometry after AO staining, and the percentages of AO^{Low} cells are shown in white, light gray, and dark gray, respectively. The graph shows the mean percentages of apoptotic cells in three independent experiments. Error bars represent the standard errors of the means. *, $P < 0.05$ by Student's *t* test comparing PV-infected and STS-treated IMR5 cells to mock-infected IMR5 cells. (C) One-step growth curve of PV in IMR5 cells. Cells and supernatants were harvested at the indicated times p.i. and subjected to three cycles of freezing and thawing. Total virus yields were determined by $TCID_{50}$ assay. Each point represents the mean virus titer for three independent experiments. Standard errors of the means are indicated. (D) Kinetics of cytopathic effect in PV-infected IMR5 cells. Cells were visualized by light microscopy at the indicated times p.i. Magnification, ×150. (E) Assessment of plasma membrane integrity. Flow cytometry histograms produced after staining of mock- and PV-infected IMR5 cells with PI at the indicated times. PI cannot enter cells with intact plasma membranes. When the plasma membranes are disrupted, cells become permeable to PI. The percentages of cells with intact membranes are indicated. Diagrams representative of two experiments are shown.

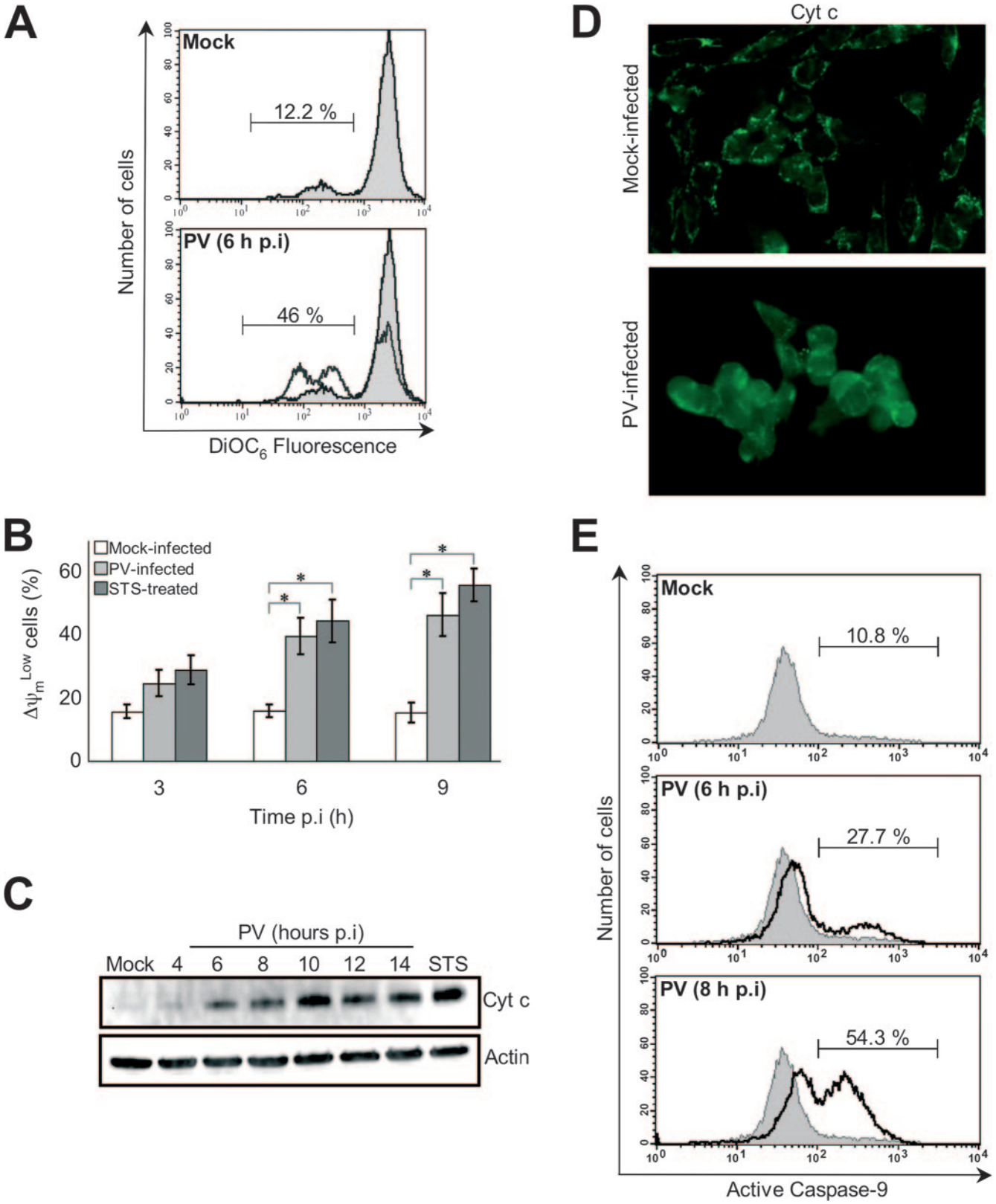

FIG. 2. PV-induced mitochondrial damage in neuronal cells. (A) Representative flow cytometric histograms after $DiOC_6$ staining of mock-infected (gray area) and PV-infected (6 h p.i.; white area) IMR5 cells. The percentages of apoptotic cells corresponding to a reduced fluorescence intensity ($\Delta\psi_m^{Low}$) for each of the two experimental conditions are indicated. (B) Flow cytometric analysis of mitochondrial-permeability transition in PV-infected IMR5 cells. Mock-infected, PV-infected, and STS-treated IMR5 cells were analyzed at the indicated times p.i. by flow cytometry after $DiOC_6$ staining, and the percentages of $\Delta\psi_m^{Low}$ cells are shown in white, light gray, and dark gray, respectively. The graph reports the mean

cells, cytochrome *c* staining displayed a dotted pattern consistent with it being restricted to mitochondria.

Cytochrome *c* release leads to the activation of initiator caspase-9 (44). We therefore assessed caspase-9 activation in PV-infected IMR5 cells at 6 h and 8 h p.i., by flow cytometry with a FLICA apoptosis detection kit, based on the specific binding of a fluorescein-labeled inhibitor (FAM-LEHD-fmk; Immunochemistry Technologies, LLC) to active caspase (Fig. 2E). Caspase-9 activation was detected from 6 h p.i.

Thus, PV-infected IMR5 cells concomitantly display MOMP, cytochrome *c* release, caspase-9 activation, and chromatin condensation and fragmentation.

Bax-mediated MOMP in PV-infected IMR5 cells. We investigated upstream signals that triggered $\Delta\psi_m$ loss in PV-infected cells. The mitochondrial pathway is regulated by the members of the Bcl-2 family, including the proapoptotic protein Bax, which promotes the release of cytochrome *c* (15). In healthy cells, most Bax is located in the cytoplasm. Bax-mediated cell death occurs through well-controlled steps, including a conformational change that exposes the NH_2 terminus of Bax and its translocation from the cytosol to mitochondria (28, 74).

We followed the translocation of Bax into mitochondria in PV-infected IMR5 cells by subcellular fractionation and Western blotting with an anti-Bax antibody (Fig. 3A). In mock-infected cells, Bax was more abundant in the cytosol, whereas in STS-treated and in PV-infected IMR5 cells, the amount of Bax in the cytosolic fraction declined with a parallel increase in the heavy membrane fraction. Thus, Bax was translocated into mitochondria in PV-infected IMR5 cells.

Then, we investigated the kinetics of the change in conformation of Bax in IMR5-infected cells. Total cell lysates were prepared at the indicated times p.i. (Fig. 3B) in a lysis buffer (containing 1% CHAPS) that did not affect Bax conformation. Bax was then immunoprecipitated with an anti-Bax antibody (6A7) that specifically recognizes Bax protein with an exposed NH_2 terminus. This antibody therefore specifically recognizes Bax in its active conformation, following exposure to proapoptotic stimuli, but does not bind to Bax in its nonactive conformation. Immunoprecipitated Bax from mock- and PV-infected cells was visualized by Western blotting (Fig. 3B, top). No activated Bax was detected in the immunoprecipitates from mock-infected cells. From 6 h p.i., Bax was immunoprecipitated with the 6A7 antibody (Fig. 3B, top), indicating that PV infection induced the change in Bax conformation as observed in the STS-treated cells used as positive controls (data not shown). We also checked that the total amount of Bax was not affected in PV-infected cells (Fig. 3B, bottom). Overall, these results indicate that PV infection triggers a change in the conformation of Bax in IMR5 cells that is concomitant with MOMP.

Bax activation was illustrated by immunofluorescence staining 6 h p.i. with another anti-Bax antibody that specifically recognizes the active form of Bax, the NT antibody. Representative staining patterns for mock-infected and PV-infected IMR5 cells are presented in the Fig. 3C. In mock-infected cells, no immunofluorescence staining was detected, whereas in PV-infected IMR5, Bax bound the NT antibody and was therefore activated, and it displayed a dotted immunofluorescence pattern in agreement with its association with mitochondria. These results demonstrate that PV infection triggers both Bax translocation from the cytosol to mitochondria and its conformational change.

We then tested whether Bax was required for PV-induced mitochondrial dysfunction. IMR5 cells were transfected with a plasmid encoding the Myc-tagged vMIA. vMIA is a cytomegalovirus-encoded cell death suppressor protein (22) that specifically neutralizes Bax (5). Untreated cells and cells transfected with empty vector pcDNA3.1 were used as negative controls. Expression of vMIA in transfected cells was assessed by Western blotting analysis with anti-Myc antibody (Fig. 3D, top). Eight hours after PV infection, cytochrome *c* release into the cytosolic fraction was reduced in cells expressing vMIA but not in pcDNA3.1-transfected cells (Fig. 3D, bottom). These results indicate that MOMP following PV infection in IMR5 cells is Bax dependent.

PV-mediated MOMP in neuronal cells is Bid and Bim independent. Given our observations on the activation of Bax, we tried to identify the PV-induced mechanism involved. Several candidates, particularly the BH3-only proteins Bid and Bim, have been proposed to activate Bax.

Bax activation can be triggered by Bid, following its cleavage by caspase-8 (43, 48). We used immunoblotting to analyze the kinetics of Bid and procaspase-8 processing in IMR5 cells following PV infection. Bid was clearly processed 14 h p.i., and the decrease in the amount of procaspase-8 suggested that caspase-8 activation occurred at the same time point (Fig. 4A, top). We confirmed caspase-8 activation in PV-infected IMR5 cells at 14 h p.i., by flow cytometry with a FLICA apoptosis detection kit, based on the specific binding of a fluorescein-labeled inhibitor (FAM-LETD-fmk; Immunochemistry Technologies, LLC) to active caspase (Fig. 4A, bottom). We found that the cells displayed caspase-8 activation at this time point, when procaspase-8 processing began to be detected (Fig. 4A, top). Thus, PV-infected IMR5 cells display concomitant

percentages of $\Delta\psi_m^{Low}$ cells obtained from three independent experiments. Error bars represent the standard errors of the means. *, $P < 0.05$ by Student's *t* test comparing PV-infected and STS-treated IMR5 cells to mock-infected IMR5 cells. (C) Time course of cytochrome *c* redistribution in PV-infected IMR5 cells. At the indicated times p.i., cells were collected and subjected to subcellular fractionation. The cytochrome *c* (Cyt c) was detected in the cytosolic fraction by Western blotting analysis with an anti-cytochrome *c* antibody. Mock-infected IMR5 cells and cells treated with STS for 8 h were used as negative and positive controls, respectively. Levels of actin were used to control for protein loading. (D) Cytochrome *c* redistribution in PV-infected IMR5 cells. Mock-infected and PV-infected IMR5 (6 h p.i.) cells were stained by immunofluorescence with a specific monoclonal antibody against cytochrome *c* and a secondary, fluorescein-conjugated antibody. See the text for details. (E) Caspase-9 activation in PV-infected IMR5 cells. Caspase-9 activation was determined in mock- and PV-infected IMR5 cells (6 h and 8 h p.i.) by flow cytometry, using a fluorescein-labeled inhibitor (FAM-LEHD-fmk) that binds specifically to active caspase-9, as described in Materials and Methods. A histogram representative of two independent experiments is shown. The percentages of cells positive for activated caspase-9 are indicated.

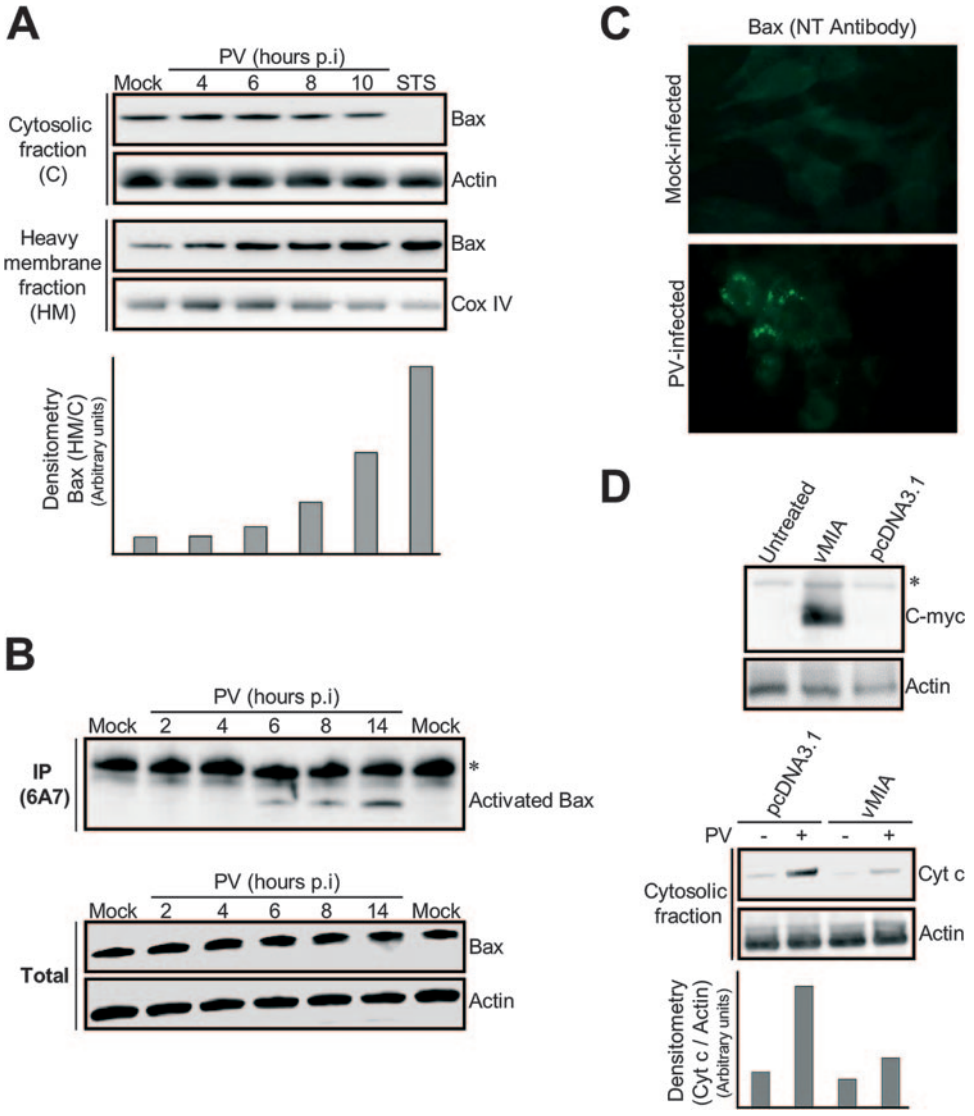

FIG. 3. PV-mediated cytochrome *c* release in neuronal cells is Bax dependent. (A) Translocation of the proapoptotic protein Bax to mitochondria in PV-infected IMR5 cells. At the indicated time p.i., equal amounts of cytosolic and mitochondrial proteins were assayed for Bax by Western blotting. Mock-infected and STS-treated (8 h posttreatment) IMR5 cells were used as negative and positive controls, respectively. Cox IV and actin were used as protein loading controls for heavy membrane and cytosolic fractions, respectively. Protein levels of heavy membrane and cytosolic fractions were determined by densitometry and plotted as ratios relative to the levels of Cox IV and actin, respectively. (B) Time course of PV-induced Bax conformational change in IMR5 cells. (Top) Mock-infected and PV-infected IMR5 cells were lysed in immunoprecipitation buffer. Conformationally active Bax protein was immunoprecipitated (IP) with anti-Bax 6A7 antibody and the precipitates were immunoblotted with anti-Bax antibody. The asterisk indicates immunoglobulin light chains. (Bottom) Whole-cell lysates that were not incubated with antibody were similarly tested for Bax by immunoblotting to check for equal amounts of Bax protein in samples prior to immunoprecipitation. Actin was used as protein loading controls. (C) PV-induced Bax activation. Mock-infected and PV-infected (6 h p.i.) IMR5 cells were analyzed by immunofluorescence with an antibody specific for the N terminus of Bax (NT antibody) to detect Bax conformational change. (D) Inhibition of cytochrome *c* release after vMIA expression in PV-infected IMR5 cells. (Top) Cells were transfected with plasmids encoding Myc-tagged vMIA, were transfected with empty vector (pcDNA3.1), or were left untreated. vMIA protein was detected in whole-cell lysates by Western blotting analysis with anti-Myc antibody. Actin was used as a protein loading control. The asterisk indicates a probable nonspecific protein band. (Bottom) Cytochrome *c* (Cyt c) release 24 h after transfection was analyzed in cytosolic fractions of mock-infected and PV-infected cells (8 h p.i.) by immunoblotting. Protein levels were determined by densitometry and plotted as ratios relative to the levels of actin.

caspase-8 activation and Bid processing. These events occurred some time after mitochondrial dysfunction (around 6 h p.i.) (Fig. 2B and C). Moreover, the treatment of PV-infected cells with the broad-spectrum caspase inhibitor z-VAD-fmk (100 μM) did not prevent cytochrome *c* release (Fig. 4B). At this concentration, z-VAD-fmk has been shown to inhibit caspases completely in cultured mammalian cells (66) without affecting PV growth (data not shown). Therefore, the processing of Bid and caspase activation, despite being induced by PV infection, do not seem to be the primary causes of the mitochondrial dysfunction in PV-infected IMR5 cells.

Bim may be transcriptionally up-regulated following apop-

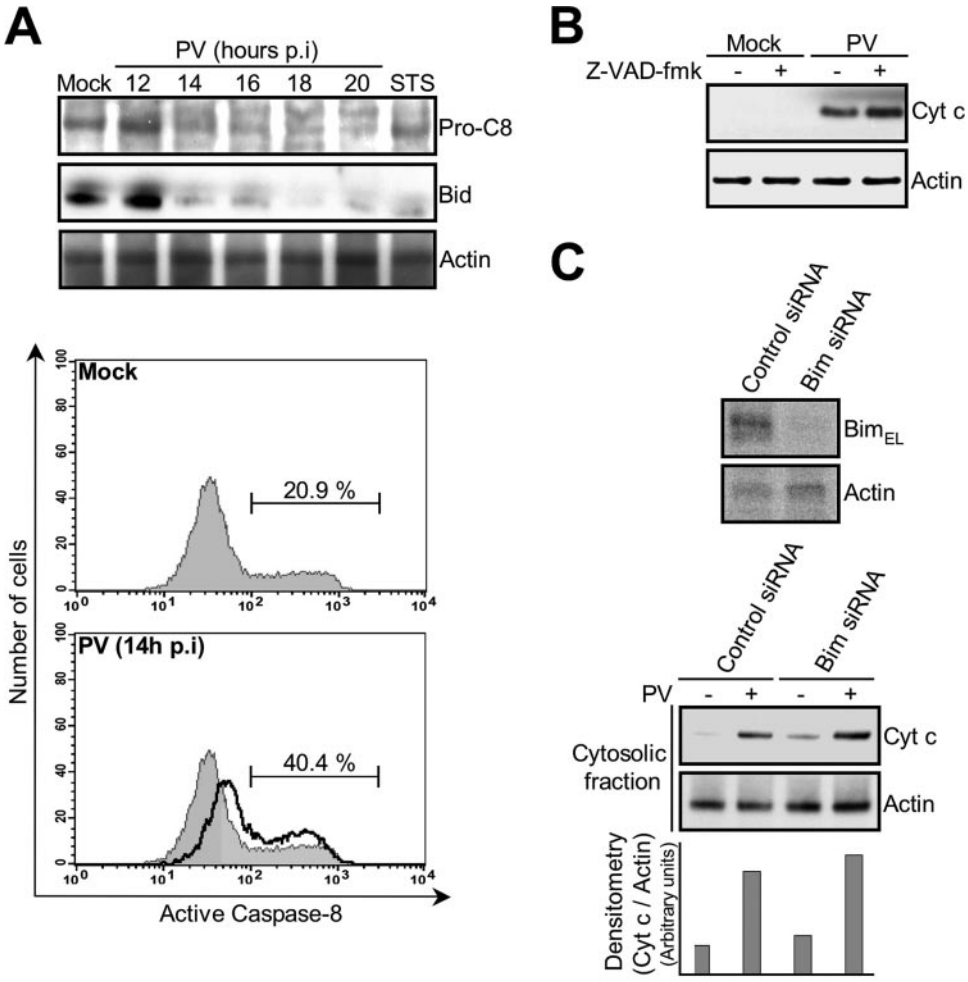

FIG. 4. PV-mediated MOMP in neuronal cells is Bid and Bim independent. (A) Time course of caspase-8 and Bid processing in PV-infected IMR5 cells. (Top) At the indicated times p.i., whole-cell extracts were subjected to immunoblot analysis with anti-caspase-8 (Pro-C8) and anti-Bid antibodies. Actin was used as a control for protein loading. (Bottom) Caspase-8 activation in PV-infected IMR5 cells. Caspase-8 activation was determined in mock- and PV-infected IMR5 cells (14 h p.i.) by flow cytometry using a fluorescein-labeled inhibitor (FAM-LETD-fmk) that binds specifically to active caspase-8, as described in Materials and Methods. Histograms representative of two independent experiments are shown. The percentages of cells positive for activated caspase-8 are indicated. (B) The broad-spectrum caspase inhibitor z-VAD-fmk does not inhibit cytochrome *c* release during PV infection. Mock- and PV-infected IMR5 cells were left untreated or treated with 100 μM z-VAD-fmk for 2 h before PV infection, and the inhibitor concentration was maintained during the adsorption period and throughout PV infection. Cytochrome *c* (Cyt c) was assayed in cytosolic extracts by Western blot analysis (14 h p.i.). Actin was used as a control for protein loading. (C) No inhibition of cytochrome *c* release after knockdown of Bim expression in PV-infected cells. (Top) IMR5 cells were transfected with Bim siRNA or nontargeted control siRNA. Bim protein was then assayed by immunoblotting with extracts from nontargeted control siRNA-transfected and Bim siRNA-transfected cells. Actin was used as a protein loading control. (Bottom) Cells were uninfected or were infected with PV 72 h after transfection, and cytochrome *c* (Cyt c) release was analyzed in cytosolic fractions by Western blotting 8 h p.i. Actin was used as a protein loading control. Protein levels were determined by densitometry and plotted as ratios relative to the levels of actin.

totic signals in neuronal cells (58). Bim can activate Bax indirectly by binding to antiapoptotic members of the Bcl-2 family (59) and can also directly bind and activate Bax (41, 49). Of the three known isoforms, Bim_{EL}, Bim_L, and Bim_S, only Bim_{EL} was detected consistently in IMR5 cells and was equally abundant in PV-infected and mock-infected IMR5 cells (data not shown). To address whether Bim_{EL} plays a major role in mitochondrial dysfunction in PV-infected cells, we down-regulated Bim_{EL} expression by using specific siRNA. Western blot analysis with a specific antibody showed that Bim_{EL} expression in IMR5 cells transfected with Bim_{EL} siRNA was significantly lower than that in those transfected with a nontargeted control siRNA (Fig. 4C, top). However, following PV infection (8 h p.i.), cytochrome *c* release in Bim_{EL} knockdown cells was not lower than that in nontargeted control siRNA-transfected cells (Fig. 4C, bottom). These results indicate that neither Bid nor Bim is a major cause of Bax-dependent cytochrome *c* release in PV-infected IMR5 cells.

Early JNK activation is required for PV-induced Bax-dependent mitochondrial dysfunction in neuronal cells. It has been recently proposed that activated JNK can stimulate Bax-dependent, stress-induced release of cytochrome *c* (39). We therefore investigated the role of JNK in mitochondrial dysfunction induced by PV in IMR5 cells.

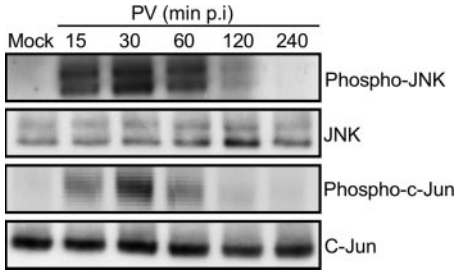

FIG. 5. Early activation of JNK and subsequent c-Jun phosphorylation in PV-infected neuronal cells. Activation of each JNK and c-Jun was analyzed in whole-cell lysates at the indicated times p.i. by Western blotting using specific anti-phospho (Thr183/Tyr185)-JNK (p46 [JNK1] and p54 [JNK2/3]) and anti-phospho (Ser63)-c-Jun antibodies. Blots were subsequently stripped and reprobed with antibodies recognizing all JNK and c-Jun forms to confirm equal protein loading.

The kinetics of JNK activation in PV-infected cells was followed by detecting phosphorylated forms of JNK by Western blotting whole-cell lysates with anti-phospho-JNK antibody. Phosphorylated JNK appeared early after PV infection (15 min), increased until 30 min p.i., and then decreased; at 4 h p.i., no phosphorylated JNK was detected (Fig. 5). Because JNK are the main upstream kinases involved in phosphorylation of NH_2-terminal c-Jun, we also tested for the functional activity of phosphorylated JNK by analyzing the phosphorylation of c-Jun with a specific antibody. Consistent with the time course of JNK activation, c-Jun phosphorylation increased to a peak at 30 min p.i. (Fig. 5). Total levels of JNK and c-Jun forms were similar at all times. JNK activation was also investigated in another human neuroblastoma cell line, SK-N-SH cells, in which JNK phosphorylation was similarly detected 30 min p.i. (data not shown).

We then investigated whether JNK activation was required for the translocation of Bax to mitochondria and the induction of cytochrome *c* release in PV-infected IMR5 cells. The specific JNK inhibitor SP600125 (25 μM) (9) was added to cells 2 h before PV infection, and was maintained during the adsorption period and throughout infection, to inhibit JNK activity. Time zero corresponds to the time of inoculation. The catalytic JNK activity was assayed by following the phosphorylation of c-Jun (Fig. 6A). SP600125 prevented the phosphorylation of c-Jun in PV-infected cells, whereas kinases upstream of JNK were not affected, given that JNK phosphorylation was not modified with SP600125.

We next investigated mitochondrial translocation of Bax in PV-infected IMR5 cells treated with SP600125. The amount of Bax was unaffected (Fig. 6B), but treatment with SP600125 strongly inhibited Bax translocation from the cytosolic fraction to the heavy membrane fraction in PV-infected cells (Fig. 6C). Similarly, SP600125 strongly inhibited cytochrome *c* release from the mitochondria into the cytosol of PV-infected IMR5 cells (Fig. 6D) but did not affect the overall abundance of this protein (Fig. 6B). Furthermore, in the presence of JNK inhibitor, there was a delay in the onset of cell layer damage in PV-infected cells, as clearly observed at the 8-h p.i. time point (Fig. 6E), with no effect on the amount of total virus produced (Fig. 6F). At later time points, cell layer damage in treated cells was similar to that in untreated cells, as shown for the 14-h p.i. time point. As there was an apparent discrepancy between the delayed destruction of infected cells in the presence of JNK inhibitor (Fig. 6E) and the absence of change in viral yield (Fig. 6F), we assessed possible effects of the delay in cell layer damage on externalization of the virus. As expected, virus release was delayed in the presence of JNK inhibitor, as observed at the 8-h p.i. time point (Fig. 6F). At later time points, no difference was observed in the level of extracellular virus between treated and untreated cells, consistent with the similar appearances of the corresponding cell layers.

Overall, these results show that PV induces JNK activation in IMR5 cells and that this early event is required for Bax translocation, MOMP, and cell death. This activation may also be involved in early viral release.

UV-inactivated PV also induces JNK phosphorylation but not apoptosis in IMR5 cells. We investigated whether PV adsorption onto IMR5 cells could induce JNK activation in the absence of PV replication by assessing JNK phosphorylation after the addition of UV-inactivated PV to IMR5 cells at a dilution corresponding to an MOI of 10 $TCID_{50}$ per cell. The complete abolition of viral infectivity by UV light treatment was confirmed by a titration assay with undiluted viral suspension. We also checked that UV inactivation did not modify virus adsorption on cells by comparing the binding efficiencies of infectious and UV light-treated PV labeled with [^{35}S]methionine (data not shown). As shown in Fig. 7A, JNK phosphorylation was induced in IMR5 cells 30 min after the addition of UV-inactivated PV, at an efficiency similar to that obtained with infectious PV. This result indicates that PV-cell receptor interaction alone is sufficient to induce JNK phosphorylation in the absence of viral replication (Fig. 7A). However, no apoptosis was detected by flow cytometry after AO staining, 8 h after the addition of UV-inactivated PV, whereas apoptosis was detected at the same time point in cells infected with infectious PV (Fig. 7B). Thus, PV-induced JNK phosphorylation is necessary, but not sufficient, to trigger apoptosis and seems to require PV postadsorption events.

DISCUSSION

Apoptosis is frequently involved in central nervous system cell damage in response to virus infection (26, 42, 64). The main target cell of PV in the central nervous system is the motor neuron resident within the spinal cord and the brain stem, and infection of these cells causes flaccid paralysis (52, 61).

Here, we demonstrated that PV infection of neuronal IMR5 cells induced the activation of the proapoptotic protein Bax, manifest by its conformational change as well as by its redistribution from the cytosol to mitochondria, concomitant with MOMP. Furthermore, PV triggered Bax-dependent mitochondrial dysfunction: vMIA protein inhibited cytochrome *c* release. However, PV-induced mitochondrial dysfunction was not prevented by the broad-spectrum caspase inhibitor z-VAD-fmk, indicating that the PV-triggered apoptotic signal is transmitted to mitochondria in a caspase-independent manner. The requirement for Bax in our model is particularly interesting because Bax protein is widely distributed in the central nervous system and has been proposed to be a major sensor of neuronal death (38). Indeed, in Bax-knockout mice,

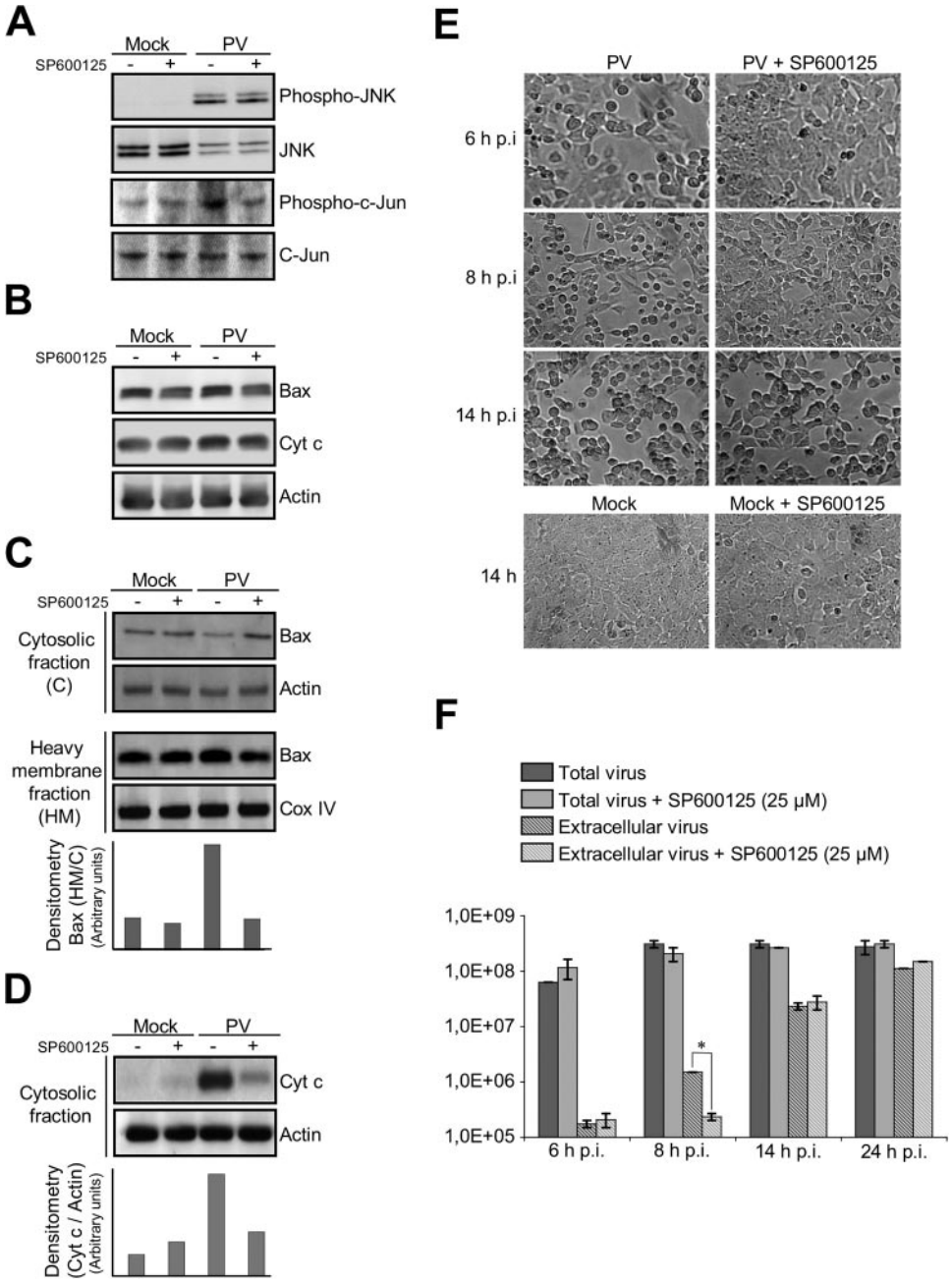

FIG. 6. Bax translocation, cytochrome *c* release, and cell death following PV infection depend on JNK activation. (A) Inhibition of JNK activity during PV infection in IMR5 cells treated with SP600125 (25 μM). Cells were incubated with the JNK inhibitor for 2 h before PV infection, and the inhibitor concentration was maintained during the adsorption period and throughout PV infection. Levels of phospho (Thr183/Tyr185)-JNK and phospho (Ser63)-c-Jun in whole-cell lysates were determined at 30 min p.i. by Western blotting. Blots were subsequently stripped and reprobed with antibodies recognizing all JNK and c-Jun forms to confirm equal protein loading. (B) IMR5 cells were uninfected or were infected with PV in the presence or absence of SP600125 (25 μM). Whole-cell lysates (8 h p.i.) were subjected to Western blot analysis with anti-Bax and anti-cytochrome *c* (Cyt c) antibodies. Actin was used as a control for protein loading. (C) Inhibition of Bax translocation from the cytosol to mitochondria by the JNK inhibitor SP600125. IMR5 cells were uninfected or were infected with PV in the presence or the absence of SP600125 (25 μM). Eight hours p.i., the cytosolic and heavy membrane fractions were assayed for Bax by Western blotting. Actin and Cox IV were used as controls for protein loading of cytosolic and heavy membrane fractions, respectively. Protein levels of heavy membrane and cytosolic fractions were determined by densitometry and plotted as ratios relative to the levels of Cox IV and actin, respectively. (D) Cytochrome *c* release is reduced by JNK inhibitor. IMR5 cells were uninfected or were infected with PV in the presence or absence of SP600125 (25 μM). Cytosolic extract proteins were analyzed at 14 h p.i. by immunoblotting with anti-cytochrome *c* (Cyt c) antibody. Actin was used as a control for protein loading. Protein levels were determined by densitometry and plotted as ratios relative to the levels of actin. (E) Inhibition of PV-induced cytopathic effect by the JNK inhibitor SP600125. Cells were uninfected or were infected with PV in the presence or absence of SP600125 (25 μM) and visualized by light microscopy at the indicated times p.i. Magnification, ×350. (F) The JNK inhibitor SP600125 does not affect PV growth but affects PV release. IMR5 cells were infected with PV in the presence or absence of SP600125 (25 μM). Total virus yield (extracellular and intracellular) was determined by $TCID_{50}$ assay at the indicated times after three cycles of freezing and thawing to release intracellular viruses. The titers of extracellular virus were determined from the supernatant of PV-infected cells at the indicated times after the removal of detached cells by centrifugation. Each point represents the mean virus titer for two independent experiments. Standard errors of the means are indicated. *, $P < 0.05$ by Student's *t* test comparing untreated IMR5 cells to treated IMR5 cells.

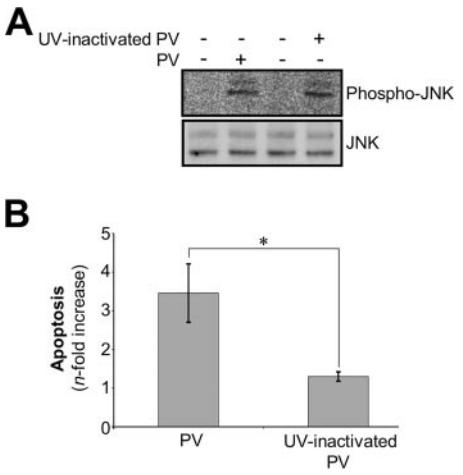

FIG. 7. UV-inactivated PV induces early JNK activation but not cell death in IMR5 cells. (A) UV-inactivated PV induces early JNK activation in IMR5 cells. JNK activation was analyzed by Western blotting whole-cell lysates from cells infected with infectious or UV-inactivated PV (30 min p.i.) with specific anti-phospho (Thr183/Tyr185)-JNK antibody. Blots were subsequently stripped and reprobed with antibodies recognizing all forms of JNK to confirm equal protein loading. (B) UV-inactivated PV did not induce cell death in IMR5 cells. Mock-infected IMR5 cells and cells infected with infectious PV or UV-inactivated PV (8 h p.i.) were analyzed by flow cytometry after AO staining and the increase (*n*-fold) in apoptosis was calculated as the ratio of the percentage of apoptotic cells among PV-infected IMR5 cells to the percentage of apoptotic cells among mock-infected IMR5 cells. Data are means from two independent experiments. Error bars represent the standard errors of the means. $*$, $P < 0.05$ by Student's *t* test comparing untreated IMR5 cells to treated IMR5 cells.

much of the postmitotic neuronal death that normally occurs in the central nervous system during development is prevented (17, 73).

Our results also provide evidence that PV activated JNK in IMR5 cells and that this event was required for Bax activation and MOMP, because SP600125—a specific pharmacological inhibitor of JNK—inhibited Bax translocation and cytochrome *c* release and delayed cell death and viral release without affecting PV replication. Thus, JNK activation may play a role in early virus release. In nonviral apoptotic models, a JNK signaling pathway has been previously described as a regulator of Bax translocation (39) and cytochrome *c* release (69). JNK can phosphorylate and activate the proapoptotic BH3-only protein Bim, leading to cell death, which is dependent upon Bax expression (39, 57). However, neither the amount nor the phosphorylation of Bim in PV-infected cells was higher than that in mock-infected cells (data not shown). Furthermore, knocking down Bim protein production with specific siRNA did not prevent cytochrome *c* release. Thus, the regulation of Bax by JNK in PV-infected IMR5 cells is independent of Bim activation.

Interestingly, the PV-cell receptor interaction alone was sufficient to induce JNK activation. The involvement of viral binding to a receptor in cell death has been demonstrated for various viruses, including reovirus (70), Sindbis virus (31), human immunodeficiency virus (40), coronavirus (45), bovine herpesvirus (27), and avian leukosis virus (11). It has been suggested that PV-CD155 interaction could induce cell death (51), and this is in agreement with results reported by Agol's group following nonpermissive infection (68). Furthermore, PV-induced apoptosis in murine L cells expressing CD155 can be modulated according to the form of CD155 expressed at the cell surface: cells expressing a CD155 form with an Ala67→Thr substitution near the binding site of CD155 for PV and corresponding to a switch from one allelic form of the PV receptor to another previously identified allelic form (36, 50) are less susceptible to PV-induced apoptosis than those expressing the Ala67 form (24). Therefore, there is the possibility, although speculative, that JNK activation is poorly efficient or delayed in cells expressing the mutated receptor.

However, as shown with UV-inactivated PV, JNK activation was not sufficient to trigger PV-induced apoptosis requiring PV replication in our model. Indeed, in addition to the PV-CD155 interaction, several nonstructural viral proteins have been implicated in the apoptotic process in PV-infected cells. The 2A and 3C proteases of PV can each trigger cellular apoptosis in the absence of other viral gene products (6, 23). However, the 3C protease may also be able to delay or prevent apoptosis, as it mediates the degradation of the transcriptional activator p53 (72). Another nonstructural protein, 3A, has an antiapoptotic activity (19, 53, 54). Thus, PV-induced apoptosis is complex and involves a delicate balance influenced by several viral and cellular proteins that may dictate the outcome for the cell.

In this study, JNK activation occurred very soon after PV infection, with a peak at 30 min p.i., and apoptotic features were first observed in PV-infected cells 6 h p.i. As previously reported by Agol's group (1), several different courses of events may occur in PV-infected cells between 30 min and 6 h p.i. These events may concern the balance between pro- and antiapoptotic viral proteins: a signal from phosphorylated JNK to the mitochondria may be transduced via an unidentified pathway involving proapoptotic viral proteins, whereas Bax activation may be delayed by cellular or viral inhibitors of apoptosis soon after PV infection.

The interaction of PV with its receptor may be the first event tipping the scale toward apoptosis in PV-infected cells. It would therefore be interesting to evaluate the involvement of the PV-CD155 interaction, particularly as concerns JNK activation, in the context of the interplay between the pro- and antiapoptotic proteins encoded by PV.

In conclusion, we demonstrated that the activation of the apoptotic mitochondrial pathway in PV-infected neuronal IMR5 cells was Bax dependent and mediated by early JNK activation. This is the first report, to our knowledge, of JNK-mediated Bax-dependent cell death associated with PV infection. These studies shed more light on the network of pathways leading to PV neuropathogenicity.

ACKNOWLEDGMENTS

We thank S. Susin and V. Yuste (Institut Pasteur, Paris, France) for the gift of IMR5 cells.

A.A. was supported by grants from the Ministère de l'Education Nationale, de la Recherche et de la Technologie. This work was supported by grants from the Institut Pasteur (PTR 120) and Danone Research, Centre Daniel Carasso.

REFERENCES

1. **Agol, V. I., G. A. Belov, K. Bienz, D. Egger, M. S. Kolesnikova, L. I. Romanova, L. V. Sladkova, and E. A. Tolskaya.** 2000. Competing death

programs in poliovirus-infected cells: commitment switch in the middle of the infectious cycle. J. Virol. **74:**5534–5541.
2. **Ammendolia, M. G., A. Tinari, A. Calcabrini, and F. Superti.** 1999. Poliovirus infection induces apoptosis in CaCo-2 cells. J. Med. Virol. **59:**122–129.
3. **Ammendrup, A., A. Maillard, K. Nielsen, N. Aabenhus Andersen, P. Serup, O. Dragsbaek Madsen, T. Mandrup-Poulsen, and C. Bonny.** 2000. The c-Jun amino-terminal kinase pathway is preferentially activated by interleukin-1 and controls apoptosis in differentiating pancreatic beta-cells. Diabetes **49:** 1468–1476.
4. **Aoki, H., P. M. Kang, J. Hampe, K. Yoshimura, T. Noma, M. Matsuzaki, and S. Izumo.** 2002. Direct activation of mitochondrial apoptosis machinery by c-Jun N-terminal kinase in adult cardiac myocytes. J. Biol. Chem. **277:**10244–10250.
5. **Arnoult, D., L. M. Bartle, A. Skaletskaya, D. Poncet, N. Zamzami, P. U. Park, J. Sharpe, R. J. Youle, and V. S. Goldmacher.** 2004. Cytomegalovirus cell death suppressor vMIA blocks Bax- but not Bak-mediated apoptosis by binding and sequestering Bax at mitochondria. Proc. Natl. Acad. Sci. USA **101:**7988–7993.
6. **Barco, A., E. Feduchi, and L. Carrasco.** 2000. Poliovirus protease 3Cpro kills cells by apoptosis. Virology **266:**352–360.
7. **Becker, E. B., J. Howell, Y. Kodama, P. A. Barker, and A. Bonni.** 2004. Characterization of the c-Jun N-terminal kinase-BimEL signaling pathway in neuronal apoptosis. J. Neurosci. **24:**8762–8770.
8. **Belov, G. A., L. I. Romanova, E. A. Tolskaya, M. S. Kolesnikova, Y. A. Lazebnik, and V. I. Agol.** 2003. The major apoptotic pathway activated and suppressed by poliovirus. J. Virol. **77:**45–56.
9. **Bennett, B. L., D. T. Sasaki, B. W. Murray, E. C. O'Leary, S. T. Sakata, W. Xu, J. C. Leisten, A. Motiwala, S. Pierce, Y. Satoh, S. S. Bhagwat, A. M. Manning, and D. W. Anderson.** 2001. SP600125, an anthrapyrazolone inhibitor of Jun N-terminal kinase. Proc. Natl. Acad. Sci. USA **98:**13681–13686.
10. **Blondel, B., F. Colbere-Garapin, T. Couderc, A. Wirotius, and F. Guivel-Benhassine.** 2005. Poliovirus, pathogenesis of poliomyelitis, and apoptosis. Curr. Top. Microbiol. Immunol. **289:**25–56.
11. **Brojatsch, J., J. Naughton, M. M. Rolls, K. Zingler, and J. A. Young.** 1996. CAR1, a TNFR-related protein, is a cellular receptor for cytopathic avian leukosis-sarcoma viruses and mediates apoptosis. Cell **87:**845–855.
12. **Choi, Y. K., T. K. Kim, C. J. Kim, J. S. Lee, S. Y. Oh, H. S. Joo, D. N. Foster, K. C. Hong, S. You, and H. Kim.** 2006. Activation of the intrinsic mitochondrial apoptotic pathway in swine influenza virus-mediated cell death. Exp. Mol. Med. **38:**11–17.
13. **Clarke, P., S. M. Meintzer, Y. Wang, L. A. Moffitt, S. M. Richardson-Burns, G. L. Johnson, and K. L. Tyler.** 2004. JNK regulates the release of proapoptotic mitochondrial factors in reovirus-infected cells. J. Virol. **78:**13132–13138.
14. **Couderc, T., F. Guivel-Benhassine, V. Calaora, A. S. Gosselin, and B. Blondel.** 2002. An ex vivo murine model to study poliovirus-induced apoptosis in nerve cells. J. Gen. Virol. **83:**1925–1930.
15. **Danial, N. N., and S. J. Korsmeyer.** 2004. Cell death: critical control points. Cell **116:**205–219.
16. **Davis, R. J.** 2000. Signal transduction by the JNK group of MAP kinases. Cell **103:**239–252.
17. **Deckwerth, T. L., J. L. Elliott, C. M. Knudson, E. M. Johnson, Jr., W. D. Snider, and S. J. Korsmeyer.** 1996. BAX is required for neuronal death after trophic factor deprivation and during development. Neuron **17:**401–411.
18. **Deng, X., L. Xiao, W. Lang, F. Gao, P. Ruvolo, and W. S. May, Jr.** 2001. Novel role for JNK as a stress-activated Bcl2 kinase. J. Biol. Chem. **276:** 23681–23688.
19. **Dodd, D. A., T. H. Giddings, Jr., and K. Kirkegaard.** 2001. Poliovirus 3A protein limits interleukin-6 (IL-6), IL-8, and beta interferon secretion during viral infection. J. Virol. **75:**8158–8165.
20. **Estaquier, J., T. Idziorek, F. de Bels, F. Barre-Sinoussi, B. Hurtrel, A. M. Aubertin, A. Venet, M. Mehtali, E. Muchmore, P. Michel, et al.** 1994. Programmed cell death and AIDS: significance of T-cell apoptosis in pathogenic and nonpathogenic primate lentiviral infections. Proc. Natl. Acad. Sci. USA **91:**9431–9435.
21. **Girard, S., T. Couderc, J. Destombes, D. Thiesson, F. Delpeyroux, and B. Blondel.** 1999. Poliovirus induces apoptosis in the mouse central nervous system. J. Virol. **73:**6066–6072.
22. **Goldmacher, V. S., L. M. Bartle, A. Skaletskaya, C. A. Dionne, N. L. Kedersha, C. A. Vater, J. W. Han, R. J. Lutz, S. Watanabe, E. D. Cahir McFarland, E. D. Kieff, E. S. Mocarski, and T. Chittenden.** 1999. A cytomegalovirus-encoded mitochondria-localized inhibitor of apoptosis structurally unrelated to Bcl-2. Proc. Natl. Acad. Sci. USA **96:**12536–12541.
23. **Goldstaub, D., A. Gradi, Z. Bercovitch, Z. Grosmann, Y. Nophar, S. Luria, N. Sonenberg, and C. Kahana.** 2000. Poliovirus 2A protease induces apoptotic cell death. Mol. Cell. Biol. **20:**1271–1277.
24. **Gosselin, A. S., Y. Simonin, F. Guivel-Benhassine, V. Rincheval, J. L. Vayssiere, B. Mignotte, F. Colbere-Garapin, T. Couderc, and B. Blondel.** 2003. Poliovirus-induced apoptosis is reduced in cells expressing a mutant CD155 selected during persistent poliovirus infection in neuroblastoma cells. J. Virol. **77:**790–798.
25. **Green, D. R., and G. Kroemer.** 2004. The pathophysiology of mitochondrial cell death. Science **305:**626–629.
26. **Griffin, D. E., and J. M. Hardwick.** 1999. Perspective: virus infections and the death of neurons. Trends Microbiol. **7:**155–160.
27. **Hanon, E., G. Meyer, A. Vanderplasschen, C. Dessy-Doize, E. Thiry, and P. P. Pastoret.** 1998. Attachment but not penetration of bovine herpesvirus 1 is necessary to induce apoptosis in target cells. J. Virol. **72:**7638–7641.
28. **Hsu, Y. T., K. G. Wolter, and R. J. Youle.** 1997. Cytosol-to-membrane redistribution of Bax and Bcl-X(L) during apoptosis. Proc. Natl. Acad. Sci. USA **94:**3668–3672.
29. **Hsu, Y. T., and R. J. Youle.** 1998. Bax in murine thymus is a soluble monomeric protein that displays differential detergent-induced conformations. J. Biol. Chem. **273:**10777–10783.
30. **Ito, T., X. Deng, B. Carr, and W. S. May.** 1997. Bcl-2 phosphorylation required for anti-apoptosis function. J. Biol. Chem. **272:**11671–11673.
31. **Jan, J.-T., and D. E. Griffin.** 1999. Induction of apoptosis by Sindbis virus occurs at cell entry and does not require virus replication. J. Virol. **73:**10296–10302.
32. **Kew, O. M., R. W. Sutter, E. M. de Gourville, W. R. Dowdle, and M. A. Pallansch.** 2005. Vaccine-derived polioviruses and the endgame strategy for global polio eradication. Annu. Rev. Microbiol. **59:**587–635.
33. **Kharbanda, S., P. Pandey, T. Yamauchi, S. Kumar, M. Kaneki, V. Kumar, A. Bharti, Z. M. Yuan, L. Ghanem, A. Rana, R. Weichselbaum, G. Johnson, and D. Kufe.** 2000. Activation of MEK kinase 1 by the c-Abl protein tyrosine kinase in response to DNA damage. Mol. Cell. Biol. **20:**4979–4989.
34. **Kharbanda, S., S. Saxena, K. Yoshida, P. Pandey, M. Kaneki, Q. Wang, K. Cheng, Y. N. Chen, A. Campbell, T. Sudha, Z. M. Yuan, J. Narula, R. Weichselbaum, C. Nalin, and D. Kufe.** 2000. Translocation of SAPK/JNK to mitochondria and interaction with Bcl-x(L) in response to DNA damage. J. Biol. Chem. **275:**322–327.
35. **Kim, S. M., J. H. Park, S. K. Chung, J. Y. Kim, H. Y. Hwang, K. C. Chung, I. Jo, S. I. Park, and J. H. Nam.** 2004. Coxsackievirus B3 infection induces cyr61 activation via JNK to mediate cell death. J. Virol. **78:**13479–13488.
36. **Koike, S., H. Horie, I. Ise, A. Okitsu, M. Yoshida, N. Iizuka, K. Takeuchi, T. Takegami, and A. Nomoto.** 1990. The poliovirus receptor protein is produced both as membrane-bound and secreted forms. EMBO J. **9:**3217–3224.
37. **Koike, S., I. Ise, Y. Sato, H. Yonekawa, O. Gotoh, and A. Nomoto.** 1992. A second gene for the African green monkey poliovirus receptor that has no putative N-glycosylation site in the functional N-terminal immunoglobulin-like domain. J. Virol. **66:**7059–7066.
38. **Krajewski, S., M. Krajewska, A. Shabaik, T. Miyashita, H. G. Wang, and J. C. Reed.** 1994. Immunohistochemical determination of in vivo distribution of Bax, a dominant inhibitor of Bcl-2. Am. J. Pathol. **145:**1323–1336.
39. **Lei, K., A. Nimnual, W. X. Zong, N. J. Kennedy, R. A. Flavell, C. B. Thompson, D. Bar-Sagi, and R. J. Davis.** 2002. The Bax subfamily of Bcl2-related proteins is essential for apoptotic signal transduction by c-Jun NH_2-terminal kinase. Mol. Cell. Biol. **22:**4929–4942.
40. **Lelièvre, J. D., F. Mammano, D. Arnoult, F. Petit, A. Grodet, J. Estaquier, and J. C. Ameisen.** 2004. A novel mechanism for HIV1-mediated bystander CD4+ T-cell death: neighboring dying cells drive the capacity of HIV1 to kill noncycling primary CD4+ T cells. Cell Death Differ. **11:**1017–1027.
41. **Letai, A., M. C. Bassik, L. D. Walensky, M. D. Sorcinelli, S. Weiler, and S. J. Korsmeyer.** 2002. Distinct BH3 domains either sensitize or activate mitochondrial apoptosis, serving as prototype cancer therapeutics. Cancer Cell **2:**183–192.
42. **Levine, B.** 2002. Apoptosis in viral infections of neurons: a protective or pathologic host response? Curr. Top. Microbiol. Immunol. **265:**95–118.
43. **Li, H., H. Zhu, C. J. Xu, and J. Yuan.** 1998. Cleavage of BID by caspase 8 mediates the mitochondrial damage in the Fas pathway of apoptosis. Cell **94:**491–501.
44. **Li, P., D. Nijhawan, I. Budihardjo, S. M. Srinivasula, M. Ahmad, E. S. Alnemri, and X. Wang.** 1997. Cytochrome c and dATP-dependent formation of Apaf-1/caspase-9 complex initiates an apoptotic protease cascade. Cell **91:**479–489.
45. **Liu, Y., Y. Cai, and X. Zhang.** 2003. Induction of caspase-dependent apoptosis in cultured rat oligodendrocytes by murine coronavirus is mediated during cell entry and does not require virus replication. J. Virol. **77:**11952–11963.
46. **Lopez, M., F. Eberle, M. G. Mattei, J. Gabert, F. Birg, F. Bardin, C. Maroc, and P. Dubreuil.** 1995. Complementary DNA characterization and chromosomal localization of a human gene related to the poliovirus receptor-encoding gene. Gene **155:**261–265.
47. **López-Guerrero, J. A., M. Alonso, F. Martin-Belmonte, and L. Carrasco.** 2000. Poliovirus induces apoptosis in the human U937 promonocytic cell line. Virology **272:**250–256.
48. **Luo, X., I. Budihardjo, H. Zou, C. Slaughter, and X. Wang.** 1998. Bid, a Bcl2 interacting protein, mediates cytochrome c release from mitochondria in response to activation of cell surface death receptors. Cell **94:**481–490.
49. **Marani, M., T. Tenev, D. Hancock, J. Downward, and N. R. Lemoine.** 2002. Identification of novel isoforms of the BH3 domain protein Bim which directly activate Bax to trigger apoptosis. Mol. Cell. Biol. **22:**3577–3589.
50. **Mendelsohn, C. L., E. Wimmer, and V. R. Racaniello.** 1989. Cellular recep-

tor for poliovirus: molecular cloning, nucleotide sequence, and expression of a new member of the immunoglobulin superfamily. Cell **56:**855–865.
51. **Morrison, M. E., Y. J. He, M. W. Wien, J. M. Hogle, and V. R. Racaniello.** 1994. Homolog-scanning mutagenesis reveals poliovirus receptor residues important for virus binding and replication. J. Virol. **68:**2578–2588.
52. **Mueller, S., E. Wimmer, and J. Cello.** 2005. Poliovirus and poliomyelitis: a tale of guts, brains, and an accidental event. Virus Res. **111:**175–193.
53. **Neznanov, N., K. P. Chumakov, A. Ullrich, V. I. Agol, and A. V. Gudkov.** 2002. Unstable receptors disappear from cell surface during poliovirus infection. Med. Sci. Monit. **8:**BR391–BR396.
54. **Neznanov, N., A. Kondratova, K. M. Chumakov, B. Angres, B. Zhumabayeva, V. I. Agol, and A. V. Gudkov.** 2001. Poliovirus protein 3A inhibits tumor necrosis factor (TNF)-induced apoptosis by eliminating the TNF receptor from the cell surface. J. Virol. **75:**10409–10420.
55. **Okuno, S., A. Saito, T. Hayashi, and P. H. Chan.** 2004. The c-Jun N-terminal protein kinase signaling pathway mediates Bax activation and subsequent neuronal apoptosis through interaction with Bim after transient focal cerebral ischemia. J. Neurosci. **24:**7879–7887.
56. **Pallansch, M., and R. Roos.** 2001. Enteroviruses: polioviruses, coxsackieviruses, echoviruses, and newer enteroviruses, p. 723–775. *In* D. M. Knipe and P. M. Howley (ed.), Fields virology, vol. 1. Lippincott Williams and Wilkins, Philadelphia, PA.
57. **Putcha, G. V., S. Le, S. Frank, C. G. Besirli, K. Clark, B. Chu, S. Alix, R. J. Youle, A. LaMarche, A. C. Maroney, and E. M. Johnson, Jr.** 2003. JNK-mediated BIM phosphorylation potentiates BAX-dependent apoptosis. Neuron **38:**899–914.
58. **Putcha, G. V., K. L. Moulder, J. P. Golden, P. Bouillet, J. A. Adams, A. Strasser, and E. M. Johnson.** 2001. Induction of BIM, a proapoptotic BH3-only BCL-2 family member, is critical for neuronal apoptosis. Neuron **29:** 615–628.
59. **Puthalakath, H., and A. Strasser.** 2002. Keeping killers on a tight leash: transcriptional and post-translational control of the pro-apoptotic activity of BH3-only proteins. Cell Death Differ. **9:**505–512.
60. **Qiao, L., S. I. Han, Y. Fang, J. S. Park, S. Gupta, D. Gilfor, G. Amorino, K. Valerie, L. Sealy, J. F. Engelhardt, S. Grant, P. B. Hylemon, and P. Dent.** 2003. Bile acid regulation of C/EBPbeta, CREB, and c-Jun function, via the extracellular signal-regulated kinase and c-Jun NH2-terminal kinase pathways, modulates the apoptotic response of hepatocytes. Mol. Cell. Biol. **23:**3052–3066.
61. **Racaniello, V. R.** 2006. One hundred years of poliovirus pathogenesis. Virology **344:**9–16.
62. **Reed, L. J., and M. Muench.** 1938. A simple method for estimating fifty percent endpoints. Am. J. Hyg. **27:**493–497.
63. **Romanova, L. I., G. A. Belov, P. V. Lidsky, E. A. Tolskaya, M. S. Kolesnikova, A. G. Evstafieva, A. B. Vartapetian, D. Egger, K. Bienz, and V. I. Agol.** 2005. Variability in apoptotic response to poliovirus infection. Virology **331:**292–306.
64. **Roulston, A., R. Marcellus, and P. E. Branton.** 1999. Virus and apoptosis. Annu. Rev. Microbiol. **53:**577–628.
65. **Ruvolo, P. P., X. Deng, and W. S. May.** 2001. Phosphorylation of Bcl2 and regulation of apoptosis. Leukemia **15:**515–522.
66. **Slee, E. A., H. Zhu, S. C. Chow, M. MacFarlane, D. W. Nicholson, and G. M. Cohen.** 1996. Benzyloxycarbonyl-Val-Ala-Asp (OMe) fluoromethylketone (Z-VAD.FMK) inhibits apoptosis by blocking the processing of CPP32. Biochem. J. **315:**21–24.
67. **Takahashi, K., H. Nakanishi, M. Miyahara, K. Mandai, K. Satoh, A. Satoh, H. Nishioka, J. Aoki, A. Nomoto, A. Mizoguchi, and Y. Takai.** 1999. Nectin/PRR: an immunoglobulin-like cell adhesion molecule recruited to cadherin-based adherens junctions through interaction with Afadin, a PDZ domain-containing protein. J. Cell Biol. **145:**539–549.
68. **Tolskaya, E. A., L. Romanova, M. S. Kolesnikova, T. A. Ivannikova, E. A. Smirnova, N. T. Raikhlin, and V. I. Agol.** 1995. Apoptosis-inducing and apoptosis-preventing functions of poliovirus. J. Virol. **69:**1181–1189.
69. **Tournier, C., P. Hess, D. D. Yang, J. Xu, T. K. Turner, A. Nimnual, D. Bar-Sagi, S. N. Jones, R. A. Flavell, and R. J. Davis.** 2000. Requirement of JNK for stress-induced activation of the cytochrome c-mediated death pathway. Science **288:**870–874.
70. **Tyler, K. L., P. Clarke, R. L. DeBiasi, D. Kominsky, and G. J. Poggioli.** 2001. Reoviruses and the host cell. Trends Microbiol. **9:**560–564.
71. **Wahid, R., M. J. Cannon, and M. Chow.** 2005. Dendritic cells and macrophages are productively infected by poliovirus. J. Virol. **79:**401–409.
72. **Weidman, M., P. Yalamanchili, B. Ng, W. Tsai, and A. Dasgupta.** 2001. Poliovirus 3C protease-mediated degradation of transcriptional activator p53 requires a cellular activity. Virology **291:**260–270.
73. **White, F. A., C. R. Keller-Peck, C. M. Knudson, S. J. Korsmeyer, and W. D. Snider.** 1998. Widespread elimination of naturally occurring neuronal death in Bax-deficient mice. J. Neurosci. **18:**1428–1439.
74. **Wolter, K. G., Y. T. Hsu, C. L. Smith, A. Nechushtan, X. G. Xi, and R. J. Youle.** 1997. Movement of Bax from the cytosol to mitochondria during apoptosis. J. Cell Biol. **139:**1281–1292.
75. **Zamai, L., E. Falcieri, G. Marhefka, and M. Vitale.** 1996. Supravital exposure to propidium iodide identifies apoptotic cells in the absence of nucleosomal DNA fragmentation. Cytometry **23:**303–311.
76. **Zu, K., L. Hawthorn, and C. Ip.** 2005. Up-regulation of c-Jun-NH2-kinase pathway contributes to the induction of mitochondria-mediated apoptosis by alpha-tocopheryl succinate in human prostate cancer cells. Mol. Cancer Ther. **4:**43–50.